Liquid crystal electric tuning of a photonic crystal laser

Brett Maune, Marko Loncar, Jeremy Witzens, Michael Hochberg, Tom Baehr-Jones, et al.

Brett Maune, Marko Loncar, Jeremy Witzens, Michael Hochberg, Tom Baehr-Jones, Yueming Qiu, Demetri Psaltis, Axel Scherer, "Liquid crystal electric tuning of a photonic crystal laser," Proc. SPIE 5511, Tuning the Optical Response of Photonic Bandgap Structures, (14 October 2004); doi: 10.1117/12.564556

SPIE.

Event: Optical Science and Technology, the SPIE 49th Annual Meeting, 2004, Denver, Colorado, United States

Liquid crystal electric tuning of a photonic crystal laser

Brett Maune*[a], Marko Loncar[b], Jeremy Witzens[a], Michael Hochberg[a], Thomas Baehr-Jones[a], Yueming Qiu[c], Demetri Psaltis[a], Axel Scherer[a]
[a]Department of Electrical Engineering and Applied Physics, California Institute of Technology, Pasadena, CA 91125, USA
[b]Division of Engineering and Applied Sciences, Harvard University, Cambridge, MA 02138
[c]In Situ Technology and Experiments Systems Section, Jet Propulsion Laboratory, California Institute of Technology, Pasadena, CA 91109, USA

ABSTRACT

We demonstrate an electrically-tuned nematic liquid crystal (LC) infiltrated photonic crystal (PC) laser. The PC laser is encased between two transparent indium tin oxide (ITO) glass plates which serve as the modulating electrodes and also define the LC cell. Applying a voltage across the cell realigns the LC, modifies the laser cavity's optical path length, and blue-shifts the lasing wavelength. The measured tuning threshold voltage agrees well with the experimentally determined LC threshold voltage which confirms the tuning is due to the LC realignment at the onset of the LC's Freedericksz transition. Furthermore, the electrically-tuned PC laser also demonstrates the successful integration of nonlinear optical materials, electronics, and fluidics with PCs and suggests further integration with other materials will lead to photonic devices with increased functionality and utility.

Keywords: photonic crystals, photonic crystal laser, liquid crystal, tunable laser

1. INTRODUCTION

It has in the past been predicted that photonic crystals will form the basis of future photonics systems. Indeed, many components of such systems have already been implemented including laser sources[1], waveguides[2], and add-drop filters[3] among others. One potential obstacle for the future debut of PC-based systems is the fabrication tolerances required for PC devices. This is particularly true for PC cavity based devices, which are created by introducing defects within the PC structure. The resonances of such cavities are extremely sensitive to the precise defect geometry and specifying *a priori* the cavity resonances of a fabricated device pushes current fabrication technology to its limits. Currently, fabricating a cavity with a specific resonance wavelength entails fabricating a large number of devices and systematically tuning fabrication parameters (e.g. electron beam writing dose). Even so, such lithographic (static) tuning techniques yield cavities with resonance resolution of several nanometers.[4] To alleviate this problem, a method to dynamically tune a cavity's resonances after fabrication is very desirable. One such method to tune PCs that has been proposed[5] and implemented to some extent[6-11] consists of infiltrating PCs with LC. Using LC to tune PC cavity resonances is plausible if the cavity mode overlaps the holes of the PC or extends into the cladding layers where the LC resides.

In this paper we present our work on electrically tuned LC infiltrated PC lasers.[12] A PC constructed from active InGaAsP material is infiltrated with a LC and is sandwiched between two transparent ITO plates, creating a LC cell around the lasers. By applying a voltage across the cell, the LC is realigned and tunes the lasing cavity. Unlike static tuning methods, this dynamic tuning scheme enables precise control of the lasing wavelength after sample fabrication. The successful integration of PC lasers within a LC cell indicates the degree to which PCs can be integrated with other technologies and suggests even further functionalization is possible. In this paper, we describe design, fabrication and measurements of LC-PC lasers. In section 2 PC cavity design, cavity tuning methodology, and LC parameter considerations are discussed; Section 3 covers experimental setups and procedures; Section 4 discusses and analyzes experimental results with comparison to simulation results, whereas Section 5 completes the paper with some discussions and conclusions.

Send correspondence to bmaune@caltech.edu

Tuning the Optical Response of Photonic Bandgap Structures, edited by Philippe M. Fauchet, Paul V. Braun, Proceedings of SPIE Vol. 5511 (SPIE, Bellingham, WA, 2004) · 0277-786X/04/$15 · doi: 10.1117/12.564556

2. PC CAVITY DESIGN, TUNING METHODOLOGY, AND LC CONSIDERATIONS

2.1. PC cavity design and tuning methodology

The PC lasers used in this work are fabricated from a 320 nm thick semiconductor slab consisting of InGaAsP quantum wells. The specifications of the quantum well material are discussed elsewhere.[13] The optical cavity is created by fabricating defects within a PC which pull defect states into the photonic bandgap of the PC (Figure 1). In-plane confinement is due to the two dimensional photonic bandgap whereas total internal reflection at the slab/cladding interface is responsible for the out-of-plane confinement.

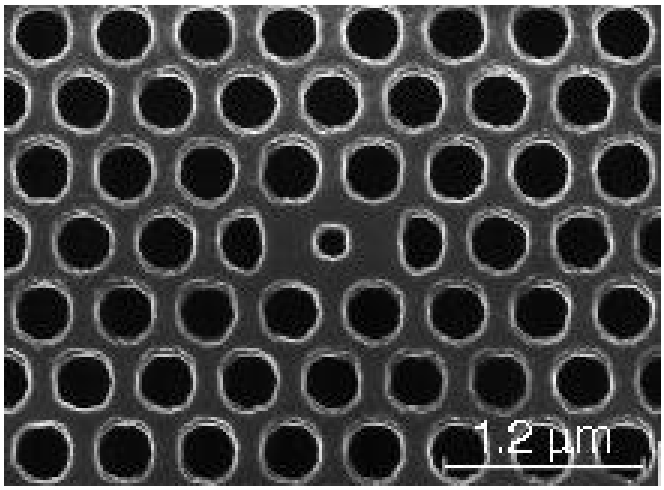

Figure 1. Scanning electron micrograph of fabricated PC laser. Periodicity of holes is 500 nm, radii of holes are 165 nm, radius of defect hole is 100 nm, slab thickness is 320 nm.

The primary cavity design criterion is to design a cavity with a sufficiently high quality factor (Q) after infiltration with LC to still enable lasing. Infiltrating the PC with LC decreases the refractive index contrast at the slab/cladding interface and reduces vertical confinement, decreasing the cavity's Q. To compensate for this, finite-difference time-domain (FDTD) simulations were used to design new high-Q cavity geometries. The resulting cavity splits the degeneracy of the orthogonally polarized X and Y dipole-like modes and maximizes the Q of the Y dipole mode (Figure 2a and 2b). FDTD simulations were used to characterize the Q of this mode as a function of the hole/cladding (ambient) refractive index. To simulate the Q, a Gaussian electromagnetic pulse was used to excite the cavity, the resulting evolving field data filtered for the frequency corresponding to the mode of interest, and the rate of energy decay within the cavity calculated. The simulated Q versus ambient refractive index is shown in Figure 3. Even though the Q is initially over 25,000 with an ambient refractive index of 1.0 corresponding to air, the Q quickly drops to approximately 2,000 as the ambient refractive index increases to 1.5, roughly the refractive index of the infiltrated LC.

After addressing the Q-dependent cavity design constraints, attention can be directed to maximizing the tunability of the laser. The PC laser is tuned by modulating the refractive index in regions that overlap with the lasing mode. The refractive index change alters the cavity's effective optical path length and shifts the resonances. To see how a cavity can be tuned with LC, one can decompose light traveling through LC into two orthogonal components. One component always experiences the LC's ordinary refractive index while the other component experiences an effective extraordinary refractive index n_{eff} given by:

$$\frac{1}{n_{eff}^2} = \frac{\sin(\theta)^2}{n_o^2} + \frac{\cos(\theta)^2}{n_e^2} \qquad (1)$$

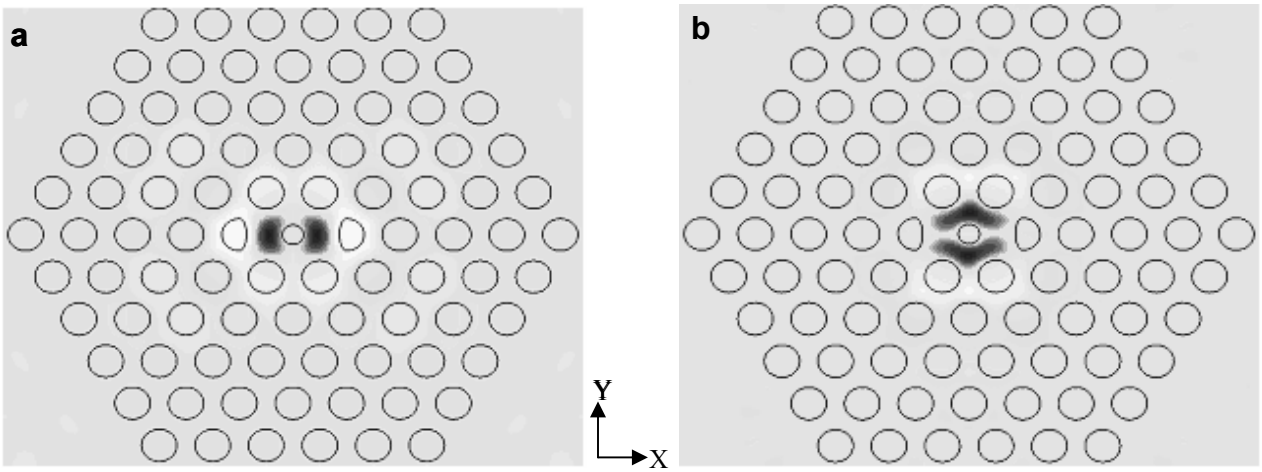

Figure 2. Z component of magnetic field for a) Y and b) X polarized dipole modes.

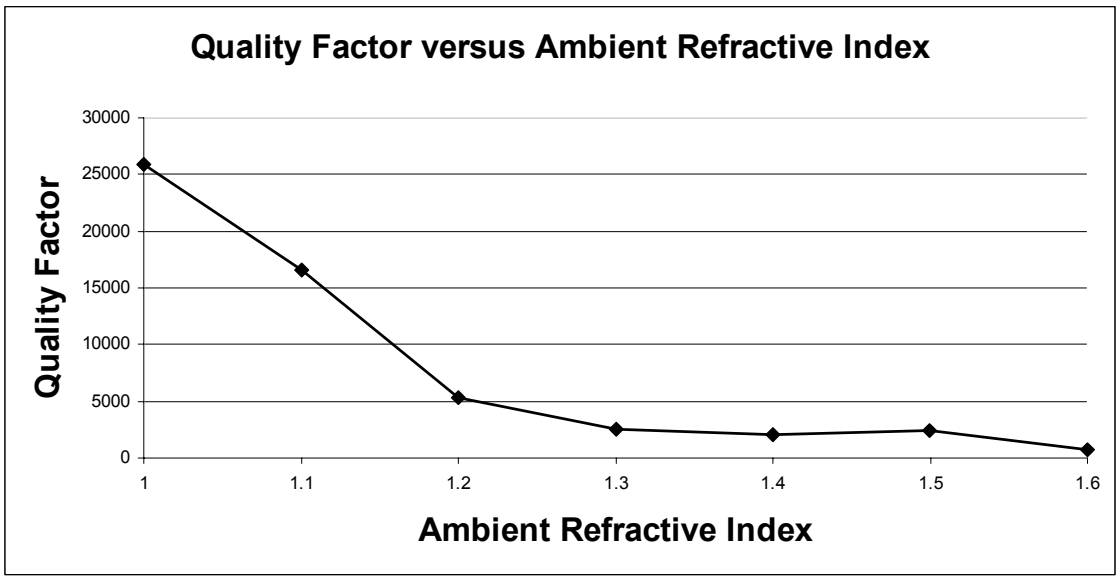

Figure 3. Quality Factor of Y dipole mode as a function of ambient refractive index. The quality factor quickly drops as the ambient refractive index increases and is around 2000 for refractive indices corresponding to that of the infiltratred LC.

where n_e and n_o are the LC's extraordinary and ordinary refractive indices, respectively, and θ is the angle between the light's polarization vector and the LC's director. Therefore by rotating the LC with respect to the cavity, n_{eff} can be changed to tune the cavity. The tuning range is limited by the refractive index modulation in the holes and the top and bottom cladding layers. Therefore, to maximize tuning, the modal overlap with these regions should also be maximized given the constraints dictated by the cavity's Q requirements. In light of this, the cavity geometry is chosen so that the optical mode's electric field maximum occurs within the central defect hole (Figure 4). Such cavities are particularly sensitive to the refractive index changes in the central hole and may be used in sensing applications.[14] In this work, FDTD simulations were used to estimate the lasing mode's sensitivity to the ambient refractive index and the results are shown in Figure 5. As expected, the photonic bandgap decreases with a reduction in refractive index contrast of the PC and the cavity resonance red-shifts to longer wavelengths as the ambient refractive index increases. For the particular

physical parameters used in the lasers presented in this work (lattice constant a = 500 nm, lasing wavelength $\lambda \approx 1.55$ μm, ambient refractive index ≈ 1.5) the tuning rate is estimated to be approximately 210 nm per unit of ambient refractive index change.

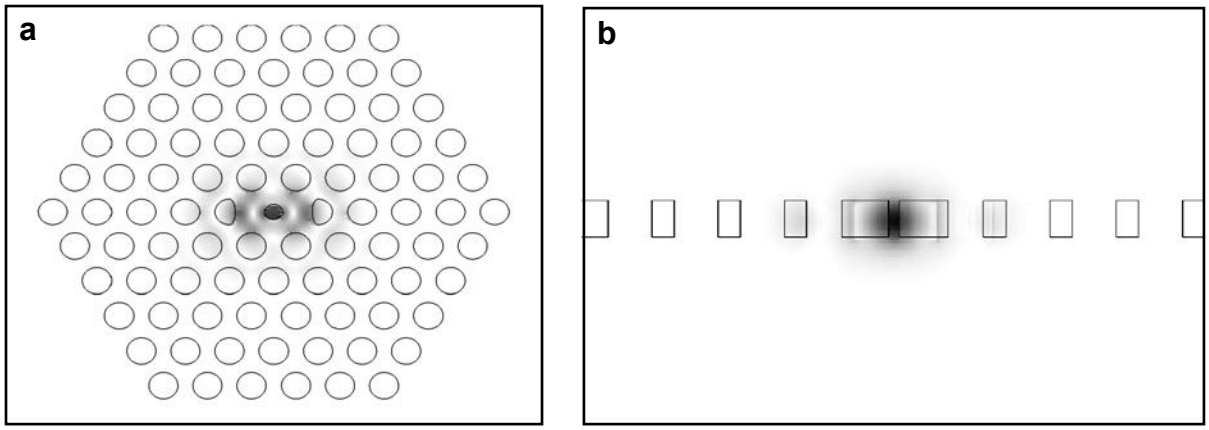

Figure 4. Top view a) and side view b) of simulated electric field amplitude for high Q Y dipole mode.

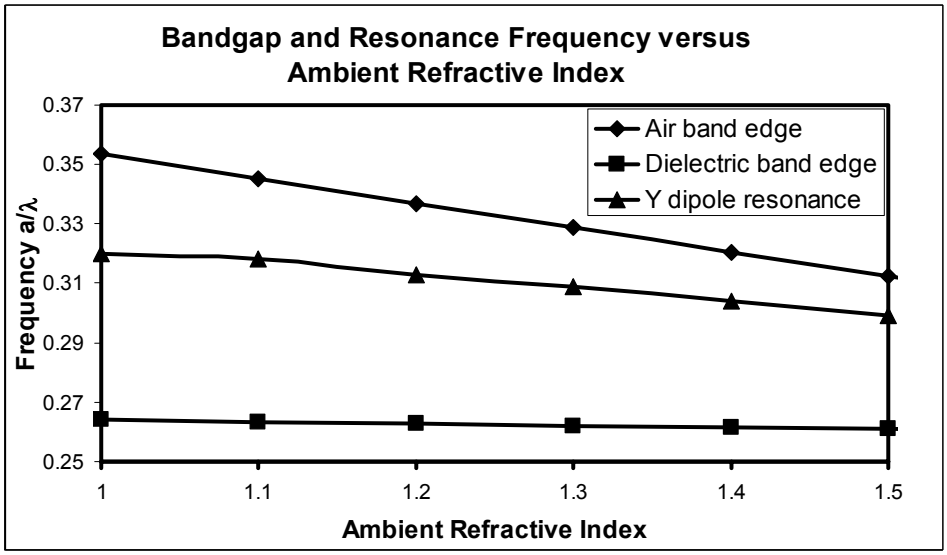

Figure 5. FDTD simulation of dielectric band, air band, and Y dipole resonance as a function of the ambient refractive index. As the ambient refractive index increases, the bandgap narrows and the resonance red-shifts. For the lasers used in this work (a = 500 nm), the tuning rate of the resonance is approximately 210 nm per unit of ambient refractive index change.

2.2. LC considerations

As mentioned previously, infiltrating the PC with LC decreases the slab/cladding refractive index contrast and decreases the vertical confinement, lowering the cavity's Q. Moreover, the LC can introduce further losses due to scattering if it is not uniformly aligned[15]—in particular within the holes of the PC. To mitigate these deleterious effects, a LC featuring the lowest refractive indices and smallest birefringence should be used. Fortunately, the birefringence of LCs tends to decrease as the refractive indices decrease and so both desirable qualities can simultaneously be realized.

Unfortunately as with the cavity design criteria, the LC selection involves a tradeoff between Q and tunability. Both the lower refractive index, which causes the lasing mode field to penetrate less into the cladding, and the smaller birefringence, which decreases the possible refractive index modulation, reduce the tuning range of the laser. For this work we chose a common LC (MLC-6815 from Merck) with a low refractive index (n_e = 1.519, n_o = 1.467 at 589 nm) and a modest birefringence (.05 at 589 nm) to maximize Q while still obtaining a detectable lasing resonance shift. Future work will investigate the use of LCs featuring larger birefringence to increase the tuning range of the lasers.

3. EXPERIMENTAL SETUP AND PROCEDURES

3.1. PC fabrication procedure and LC cell construction

The PC lasers are constructed within InGaAsP quantum well material designed to have a maximum gain at 1.55 μm. The fabrication procedure involves a combination of electron beam lithography, dry etching, and wet etching processes, and details of the processing steps have previously been described.[13]

To construct a LC cell around the PC lasers, the PC sample is first glued along with two spacers to a transparent conducting indium tin oxide (ITO) glass plate which serves as the bottom electrode. Next, a drop of LC is placed onto the PC sample. A second ITO plate is then glued to the spacers, and the resulting gap between the top ITO plate and the PC sample is approximately 15 μm. The ITO plates are chosen to minimize absorption at 1.55 μm and feature 92% transmission at that wavelength. The LC cell is then heated above the LC's clearing point (67°C) on a hotplate at 90°C for 5 minutes to help ensure complete infiltration into the PC. Wires are then attached to the ITO plates with conducting tape which are then connected to a power supply. A schematic of a completed cell is shown in Figure 6.

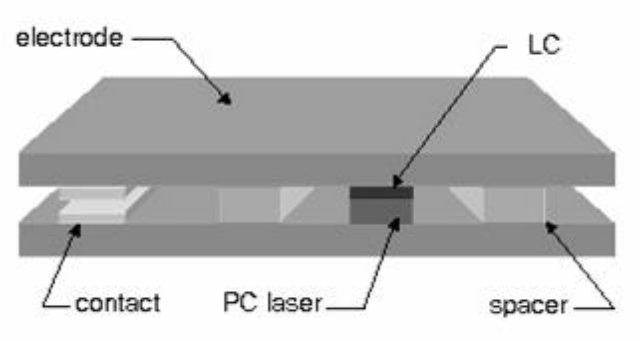

Figure 6. Cross-section of PC LC cell.

3.2. PC laser measurement and procedure

Samples are measured using a home-built micro-photoluminescence system as shown in Figure 7.[13] The samples are pumped with 4.4 mW using an 830 nm laser diode with a pulse length of 15 ns and a periodicity of 1.5 μs. Pump light is focused onto the sample using a 100x microscope objective lens. The emitted light from the cavities is then collected through the objective lens and directed into an optical spectrum analyzer (OSA) to record the spectra. A polarizer is also occasionally inserted in front of the OSA to test the polarization properties of the emitted light. Spectra are acquired while adjusting the voltage applied across the LC cell. These spectra are analyzed to determine the tuning characteristics of the lasers.

Lasing of the PC cavities can be confirmed by recording a characteristic L-L curve as shown in Figure 8. The measured threshold of approximately 2.3 mW for the LC infiltrated cavity is significantly higher than thresholds from similar cavities without LC infiltration.[16] The higher threshold after infiltration is attributed to increased losses associated primarily to decreased confinement. Further losses are introduced by scattering from nonuniformly aligned LC and also due to the LC coupling, through polarization rotation, photons out of the TE-polarized lasing mode.

3.3. LC characterization

The refractive indices of the LC used in this work are only specified at the LC industry standard 589 nm and not at the relevant wavelengths of 1.55 μm. To characterize the LC at infrared wavelengths, we infiltrate PC lasers with the

LC and compare the resonance shifts to the shifts obtained infiltrating the same cavities with index-matched fluids. The uncertainty of this method is dominated by the fact the LC orientation in the PC is not known. In theory the ambient refractive index experienced by a cavity due to the LC can range anywhere from n_o to n_e, but most likely the surface anchoring governed LC orientation yields an effective ambient refractive index far from either extreme. Within this method's resolution, the experiments indicate the LC's refractive indices, and by extension the birefringence, to be the same at 1.55 μm as at visible wavelengths.

Polarization interference microscopy (PIM) is used to further characterize the LC and serves to cross check the laser tuning data. In this method, an interference pattern is generated by imaging a birefringent sample with white light using crossed polarizers. The interference pattern yields information pertaining to the in-plane birefringence of the sample. Using this method with the LC-clad PC samples provides information about the orientation of molecules in the bulk LC above the PC cavities.[17]

PIM proved to be a valuable technique for characterizing the LC behavior both with and without the presence of an applied electric field. The LC behavior was studied by observing the interference pattern, and hence the LC orientation, as a function of voltage applied across the cell. The existence of a Freedericksz transition was verified by observing a dramatic change in the interference pattern when slowly ramping up the DC voltage applied across the cell. The corresponding threshold voltage was determined to be approximately 4V. As the voltage was increased beyond threshold, the LC increasingly aligned itself parallel to the field and normal to the PC sample. PIM was also effective in determining the saturation voltage to be approximately 8V, the voltage above which the bulk LC is essentially completely aligned parallel to the electric field.

The PIM results also demonstrate that with zero electric field the LC spontaneously aligns itself parallel (homogenously) to the PC surface even without the presence of an alignment layer. Furthermore, the homogenously oriented LC forms micron-scale domains whose directors are rotated with respect to each other. Lastly, by repeatedly cycling the voltage between zero and saturation, the PIM interference pattern always returns to the same configuration which suggests the LC exhibits surface alignment memory resulting from surface anchoring. The bulk LC orientation is probably dictated by the LC orientation at either the PC or the top electrode surface, and experiences surface anchoring which locks it into a stable configuration at the surfaces. This orientation then propagates through the bulk LC in the cell.

Unfortunately, the PIM technique only reveals direct information about the bulk LC orientation and as such does not reveal whether or not the bulk LC orientation is due to the anchored LC at the PC surface, electrode surface, or both. With that said, however, the planar geometries of the PC slab and the ITO plate favor a homogenous LC orientation and the PIM data suggest neither surface is anchored vertically (homeotropically). Therefore, the LC is believed to be primarily oriented homogenously in the vicinity of the PC slab.

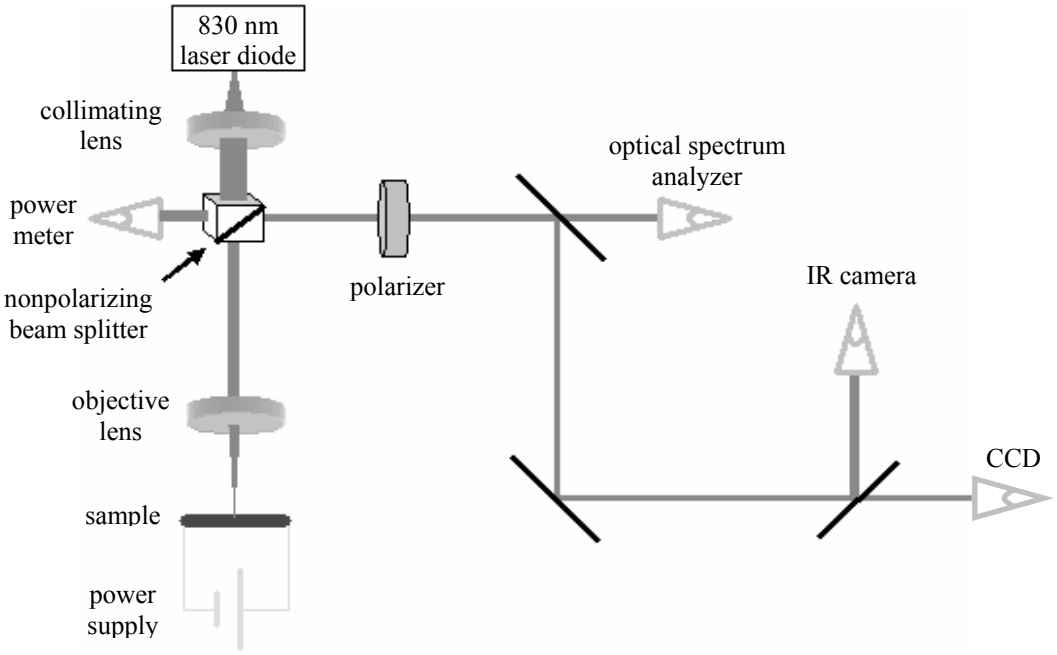

Figure 7. Schematic of PC laser testing experimental setup.

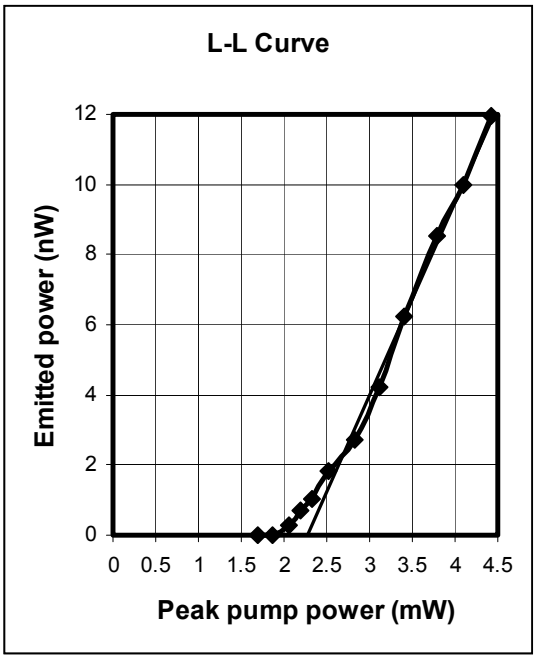

Figure 8. L-L curve taken of PC laser cavity after LC infiltration (pump pulse 15 ns and period 1.5 μs). The lasing threshold is estimated to be approximately 2.3 mW (linear fit). The relatively high threshold is attributed to increased losses associated with the LC infiltration process.

4. EXPERIMENTAL RESULTS AND ANALYSIS

4.1. Tuning and simulation results

During the optical pumping of the PC cavities, the LC is reoriented and the laser tuned by application of an electrostatic field between the top ITO electrode and the InP wafer substrate. The anticipated tuning range strongly depends on the LC's refractive indices and the birefringence at the lasing wavelength λ~1.55 μm, the zero-field LC orientation, the overlap between the lasing mode and the LC, and the electric field pattern generated by the electrodes. For the sake of establishing a baseline for the laser tuning range, the LC is assumed to have a spontaneous random orientation. The influence of the applied voltage on the LC orientation is modeled using electrostatic simulations of the generated electric field patterns (Figure 9a and 9b). These simulations indicate the LC in the top cladding layer can be aligned vertically, but the electric field is sharply damped in the holes of the PC due to the screening by the conducting PC membrane. Fortunately, the lasing mode features an evanescent field which extends into the cladding layers and is influenced by the refractive index in those regions. Therefore tuning of the laser can be achieved by changing the refractive index in the top cladding layer.

To demonstrate LC tuning of the PC lasers we record lasing spectra as a function of the gate voltage applied across the cell. The electrostatic simulations predict the LC in the top cladding should align vertically to the surface, lowering the refractive index from 1.485 to 1.467 and blue-shifting the lasing wavelength. Such a blue-shift is observed upon ramping the gate voltage from 0 to 20 V (Figure 10a). The tuning starts at approximately 4 V, in agreement with the observed threshold voltage using PIM, and signals the onset of the Freedericksz transition.[18] In Figure 10 a maximum blue-shift of approximately 1.2 nm is observed at 20 V but larger tuning ranges of nearly 2 nm have also been obtained using similar device geometries. The magnitude of the tuning range suggests only the LC in the top cladding layer is being aligned to the field, a topic discussed further below. This tuning is independent of the DC field polarity, although, a slight hysteresis can be observed which may be attributed to charging and impurity effects in the LC (Figure 10b).

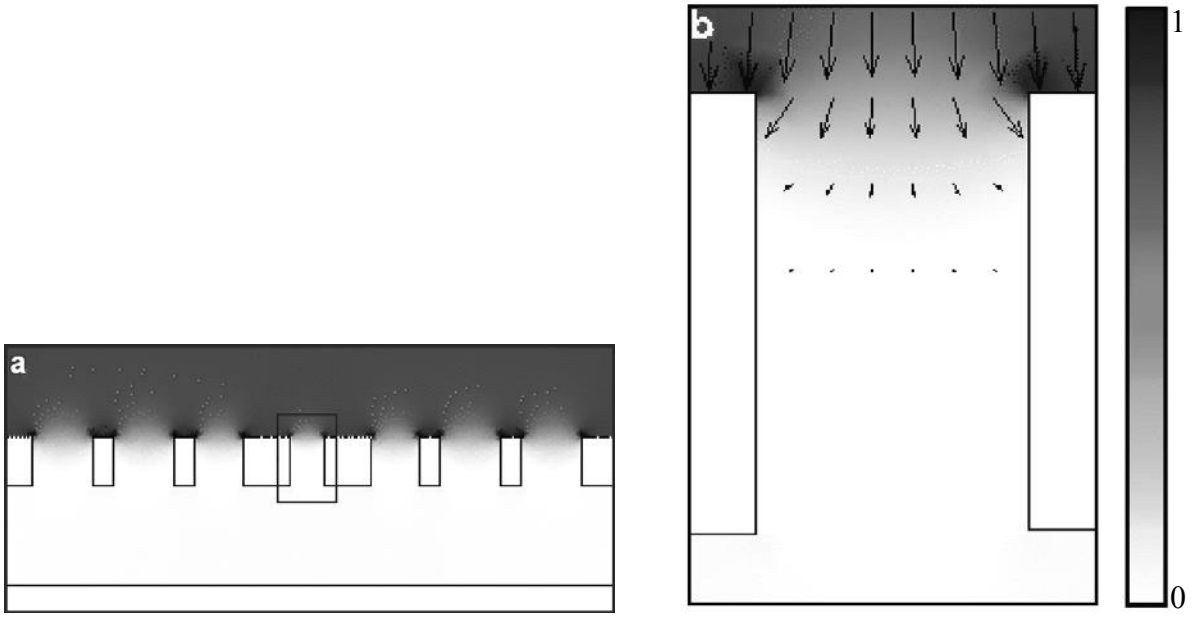

Figure 9. a) Cross-section of PC membrane showing magnitude of simulated electric field generated by ITO electrodes. b) A close-up of the generated electric field in the defect hole. Arrow direction and length denote field direction and amplitude, respectively. Field magnitudes are represented by a normalized gray scale from 0 to 1.

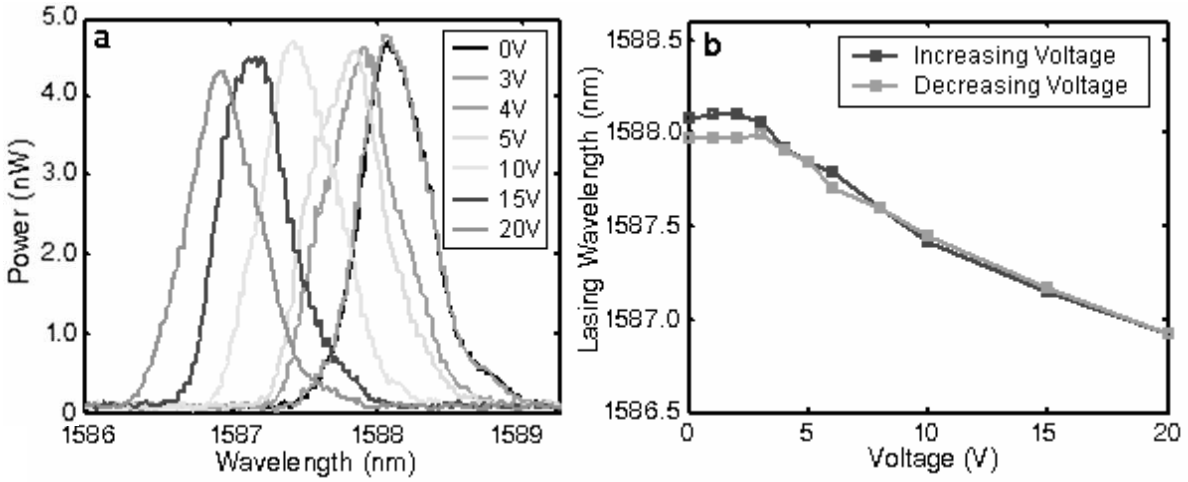

Figure 10. Demonstration of laser tuning via LC realignment. a) Laser spectra taken with an applied voltage ranging from 0-20 V across the LC cell. The threshold for tuning is approximately 4 V, coinciding with the measured LC threshold voltage using PIM. A maximum blue-shift of 1.2 nm is measured at 20 V. For clarity note lasing wavelength monotonically decreases with increasing voltage with the 0 V trace being the far right and the 20 V trace being the far left. b) Lasing wavelength versus applied voltage for a voltage ramp cycle. Although the tuning rate lessens at higher voltage, the data suggest saturation is not even reached at 20 V and further tuning may be possible with stronger fields. The tuning is reversible but demonstrates a slight hysteresis at low fields which may be due to charging or impurity effects. The marker box height represents the upper bound of the uncertainty in the lasing wavelength obtained from the spectra.

4.2. Effect of LC domain orientation on the PC tuning range

The PC cavity modes exhibit in-plane electric field components and the X and Y dipole-like modes are also primarily polarized in the x and y directions, respectively. The effective refractive index experienced by the high-Q Y dipole mode due to the LC is dependent upon the orientation of the LC with respect to the mode's polarization axis as seen by equation 1.

If the LC spontaneously forms homogenously oriented domains as the PIM data suggest, then equation 1 implies a variability of laser tuning range based upon the orientation of the domains with respect to the polarization axis of the lasing mode (Figure 11a and 11b). The tuning range is dependent upon the effective refractive index difference from the zero-field state to the saturated state. The zero-field refractive index is a function of the domain orientation but the saturated refractive index is always the same, n_o. So maximum tuning is expected when the refractive index is initially n_e and is switched to n_o. This can occur when the LC domain is initially oriented such that the LC directors are aligned parallel to the mode's polarization axis. Conversely, minimum tuning is expected when the domain is initially aligned perpendicular to the mode's polarization axis. The observed distribution in tuning range data suggests that this is indeed the case.

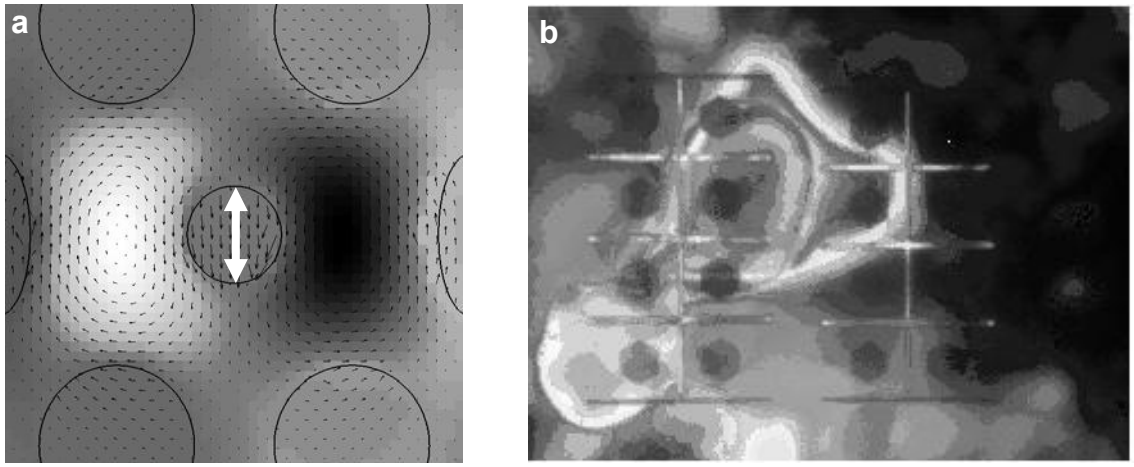

Figure 11. a) Close-up of Y dipole mode showing polarization structure. White arrow denotes dominant polarization direction. b) Interference pattern captured using PIM showing the LC spontaneously forming domains above PC lasers (hexagons).

4.3. Effect of surface anchoring and PC tuning range

The surface anchoring experienced by the LC at the ITO and PC slab interfaces locks the crystal into a stable configuration. One of the manifestations of the surface stabilization is that the LC exhibits surface alignment memory. Upon cycling the voltage between zero and saturation, the LC returns to its original configuration set by the boundary conditions. Both the tuning and PIM data indicate this reversibility is occurring. The stable configuration experienced by the nematic state can be destroyed, however, by heating the LC above its clearing point and into the isotropic state. Upon cooling and condensing back into the nematic state, the LC settles into a different stable configuration. This is confirmed by measuring different tuning ranges for the same lasers after thermal cycling and also by observing a different PIM interference pattern of the bulk LC.

Beyond stabilizing the tuning behavior of the lasers, LC anchoring to the surface of the PC slab inhibits their tuning range. As expected, the surface anchoring heavily influences the alignment dynamics of the LC in the vicinity of the PC membrane—where the lasing mode's evanescent field is strongest. The surface anchoring inhibits the LC from aligning along the electric field and thus decreases the tuning of the laser. The effects of the surface anchoring are the most pronounced for LC closest to the PC membrane. As the gate voltage is increased, LC molecules progressively closer to the PC membrane surmount the free energy barrier and align along the field. This progressive alignment explains the continued tuning of the lasers even far above the saturation voltage (Figure 12). Although the surface anchoring inhibits overall tuning, a benefit is that it enables the lasers to be continuously tuned over a range of wavelengths. Unlike other tuning methods, such as lithographic tuning, LC tuning enables Angström or even sub-Angström precision in the control of the lasing wavelength.

Two outstanding questions are the zero-field LC orientation and the degree of LC alignment in the PC holes. The electrostatic simulations indicate the field is screened from the holes, which limits the ability to control the alignment there. More importantly, however, is that the LC likely experiences anchoring to the inner walls of the holes and is amplified by confinement effects. LC in similar confined geometries have been studied and found to experience relatively strong surface anchoring and feature a homeotropic or escaped radial orientation amongst others.[6,19,20] As a result, even if the electric field penetrated the PC holes, the LC may still not align appreciably to the field but remain stationary. FDTD simulations of the expected tuning range of the lasers support the premise that negligible alignment occurs within the PC holes and is confined to the top cladding layer. For example simulations predict a blue-shift of 1 nm for an initially randomly oriented LC but with only the top cladding switching to a vertical orientation. As discussed previously, the tuning range is increased when the LC in the top cladding layer is initially oriented such that its director is aligned parallel to the lasing mode's polarization axis. For this case the simulated tuning range increases to 2 nm. The tuning range sharply increases, however, if the LC in the holes aligns with the field. FDTD simulations predict a tuning of 6 nm when both the holes and top cladding are aligned from a random state. Therefore the tuning data suggests only the top LC cladding layer is aligning to the field.

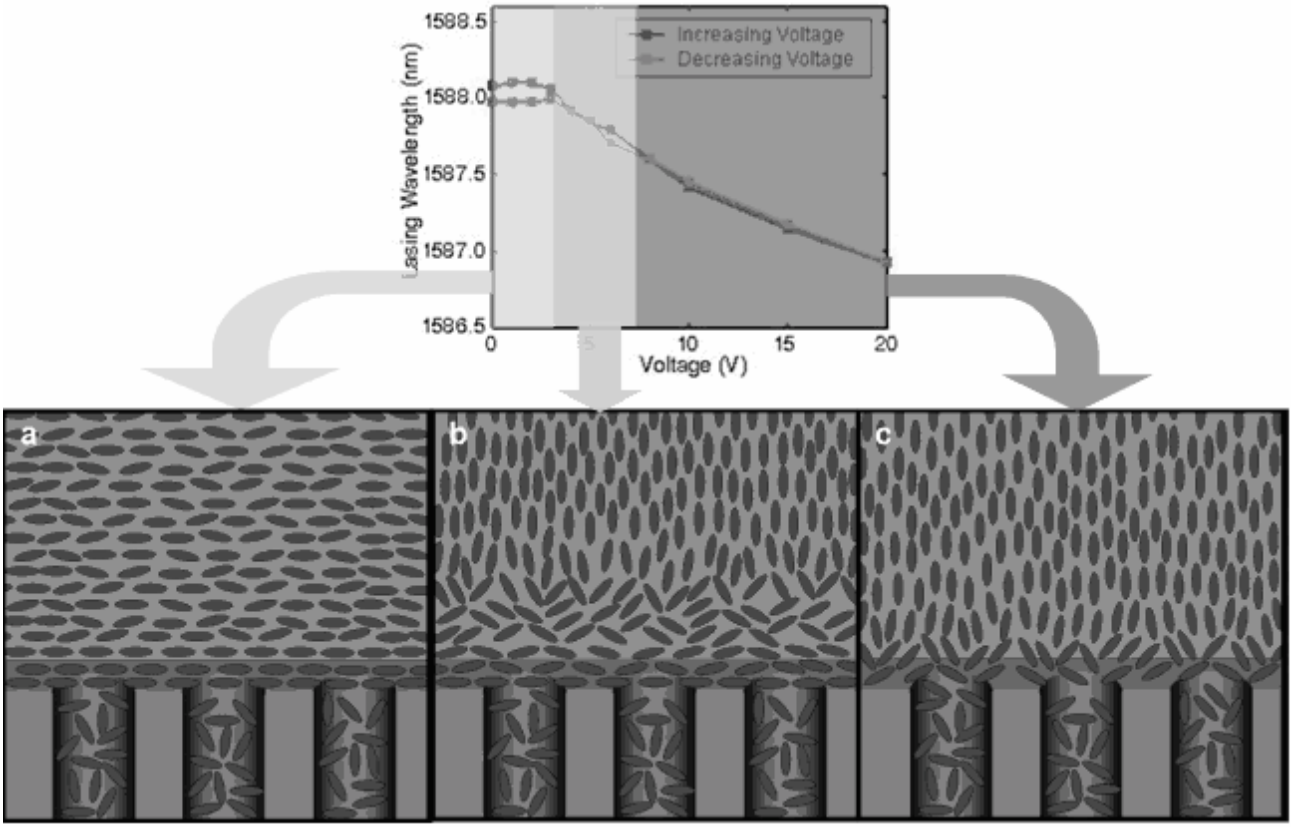

Figure 12. Presumed LC orientation at three different field regimes. a) LC oriented homogenously below threshold. b) Bulk LC aligning parallel to field above threshold. c) Above saturation voltage LC progressively closer to the PC membrane aligns parallel to field. Note LC in holes is drawn with a random orientation for convenience. The actual orientation within the holes is not known.

5. DISCUSSIONS AND CONCLUSIONS

We have fabricated and demonstrated LC infiltrated electrically tunable PC lasers. These PC lasers were fabricated from a slab containing active InGaAsP quantum wells by using electron beam lithography followed by several etching steps. The PC cavity geometry and LC were chosen to maximize the Q of one of the cavity's dipole modes after

LC infiltration. A cell was constructed around the laser sample with transparent conducting ITO plates as the modulating electrodes. The tuning behavior and LC orientation dynamics were characterized by recording laser spectra while adjusting the gate voltage across the cell and also by analyzing interference patterns obtained with PIM. Electrostatic simulations indicate the conducting PC slab screened the applied electric field and the field did not significantly penetrate the holes of the PC. The minimal electric field, surface anchoring, and confinement effects experienced by the LC within the holes suggest the LC orientation could only be controlled in the top cladding layer. The observed laser tuning ranges in conjunction with FDTD simulations of the expected tuning range support this assertion. Furthermore, by studying interference patterns using PIM we discovered the LC in the top cladding layer spontaneously formed homogenously oriented domains. Simulations indicate the lasers' tuning ranges to be dependent upon the relative orientation of the LC domains to the lasing modes' polarization axis. Experimental results of laser tuning ranges and PIM interference patterns obtained through thermal cycling the LC between nematic and isotropic states support this link. Lastly, the absence of a tuning saturation is believed to be due to the LC anchoring to the PC slab. Although surface anchoring inhibits the overall tuning range of the lasers, an advantageous side effect is that it enables continuous and precise tuning of the lasing wavelength.

The demonstration of an LC infiltrated electrically tuned PC laser is significant in several respects. First of all, incorporating various device optimizations can significantly increase the tuning range of the lasers—perhaps by an order of magnitude or more—and enable the lasers to be used in future lightwave systems, spectroscopic applications, and others. Possibilities for increasing the tuning range include designing a higher Q cavity which could enable the usage of a wide assortment of LCs featuring larger birefringence, using more efficient electrode geometries to enhance the control over the LC orientation, or by using an alignment layer to control the LC zero-field orientation. In particular, if the surface anchoring and confinement effects could be reduced in the holes, then the orientation of the LC in the top cladding layer may be able to propagate through the PC holes and thus dramatically increase the tuning range. Beyond an electrically tunable laser, these structures also provide a platform to probe the behavior of LCs confined in nanoscale geometries while enabling the simultaneous study of a LC's nonlinear optical interaction with an intense optical field. Furthermore, the successful integration of electronics and fluidics with PC lasers demonstrates the flexibility of these structures and suggests that even further functionalization is achievable.

ACKNOWLEDGEMENTS

The authors would like to thank Mark Adams, David Barsic, Rhys Lawson, Xu Wang, and Tomoyuki Yoshie for valuable discussions. Funding for this work by Jag Shah from DARPA under the CS-WDM program (Contract No. N00421-02-D-3223) is also gratefully acknowledged.

REFERENCES

1. O. Painter, R. K. Lee, A. Scherer, A. Yariv, J. D. O'Brien, P. D. Dapkus, and I. Kim, Two-dimensional photonic band-gap defect mode laser. *Science*, **284**, 1819 (1999).
2. M. Loncar, D. Nedeljkovic, T. Doll, J. Vuckovic, A. Scherer, and T. Pearsall, Waveguiding in planar photonic crystals. *Appl. Phys. Lett.*, **77**, 1937 (2000).
3. S. Noda, A. Chutinan, and M. Imada, Trapping and emission of photons by a single defect in a photonic bandgap structure. *Nature*, **407**, 608 (2000).
4. O. Painter, A. Husain, A. Scherer, P. T. Lee, I. Kim, J. D. O'Brien, and P. D. Dapkus, Lithographic tuning of a two-dimensional photonic crystal laser array. *IEEE Photonics Technol. Lett.* **12**, 1126 (2000).
5. K. Busch and S. John, Liquid-crystal photonic-band-gap materials: the tunable electromagnetic vacuum. *Phys. Rev. Lett.* **83**, 967 (1999).
6. S. W. Leonard et al. Tunable two-dimensional photonic crystals using liquid-crystal infiltration. *Phys. Rev. B* **61**, R2389, (2000).
7. G. Mertens, T. Roder, R. Schweins, K. Huber, and H. S. Kitzerow, Shift of the photonic band gap in two photonic crystal/liquid crystal composites. *Appl. Phys. Lett.* **80**, 1885, (2002).
8. C. Schuller, F. Klopf, J. P. Reithmaier, M. Kamp, and A. Forchel, Tunable photonic crystals fabricated in III-V semiconductor slab waveguides using infiltrated liquid crystals. *Appl. Phys. Lett.* **82**, 2767, (2003).

9. D. Kang, J. E. Maclennan, N. A. Clark, A. A. Zakhidov, and R. H. Baughman, Electro-optic behavior of liquid-crystal-filled silica opal photonic crystals: effect of liquid-crystal alignment. *Phys*. *Rev*. *Lett*. **86**, 4052 (2001).
10. Y. Shimoda, M. Ozaki, and K. Yoshino, Electric field tuning of a stop band in a reflection spectrum of synthetic opal infiltrated with nematic liquid crystal. *Appl*. *Phys*. *Lett*. **79**, 3627, (2001).
11. R. Ozaki, T. Matsui, M. Ozaki, and K. Yoshino, Electrically color-tunable defect mode lasing in one-dimensional photonic-band-gap system containing liquid crystal. *Appl*. *Phys*. *Lett*. **82**, 3593, (2003).
12. B. Maune, M. Loncar, J. Witzens, M. Hochberg, T. Baehr-Jones, D. Psaltis, A. Scherer, and Y. Qiu, Liquid-crystal electric tuning of a photonic crystal laser. *Appl. Phys. Lett.* **85**, 360, (2004).
13. M. Loncar, T. Yoshie, A. Scherer, P. Gogna, and Y. Qiu, Low-threshold photonic crystal laser. *Appl*. *Phys*. *Lett*. **81**, 2680, (2002).
14. M. Loncar, A. Scherer, and Y. Qiu, Photonic crystal laser sources for chemical detection. *Appl. Phys. Lett.* **81**, 4648, (2003).
15. S. Kumar, in *Liquid Crystals*, (Cambridge University Press, New York, 2001) chap. 6.
16. M. Loncar, M. Hochberg, A. Scherer, and Y. Qiu, High quality factors and room-temperature lasing in a modified single-defect photonic crystal cavity. *Opt. Lett.* **29**, 721, (2004).
17. S. Kumar, in *Liquid Crystals*, (Cambridge University Press, New York, 2001) chap. 2.
18. L. Blinov, in *Handbook of Liquid Crystals*, D. Demus, J. Goodby, G. W. Gray, H. W. Spiess, V. Vill, Eds. (Wiley-VCH, New York, 1998) vol. 1, chap. 9.
19. G. P. Crawford, M. Vilfan, J. W. Doane, and I. Vilfan, Escaped-radial nematic configuration in submicrometer-size cylindrical cavities: Deuterium nuclear-magnetic-resonance study. *Phys*. *Rev*. *A* **43**, 835, (1991).
20. G. P. Crawford, D. W. Allender, J. W. Doane, M. Vilfan, and I. Vilfan, Finite molecular anchoring in the escaped-radial nematic configuration: a ^{2}H-NMR study. *Phys*. *Rev*. *A* **44**, 2570, (1991).